Achieving Reliable U-Shift Capsule Coupling: A Comparative Study of Geometric Steering Controllers and Safe Operating Zone Determination

Raghava Santhan Mysore Pavan[a]
Institute of Vehicle Concepts, German Aerospace Center (DLR), Pfaffenwaldring 38-40, 70569 Stuttgart, Germany

Keywords: Autonomous Modular Vehicle (AMV), Coupling, Hybrid A* Path Planning, Pure Pursuit, Stanley Controller, Collision Avoidance.

Abstract: This paper presents a simulation-based comparative study of two geometric controllers, Pure Pursuit and Stanley, applied to the coupling process of an Autonomous Modular Vehicle (AMV) known as U-Shift. The maneuver involves the diveboard reversing to dock and connecting with a transport capsule. The Hybrid A* planner considers driveboard and capsule geometric constraints to generate the reference path. The study compares the controllers' performance and shows how changes in parameters and alignment between the driveboard and capsule affect coupling success rates without collisions. The paper further categorized the initial position and orientation of the diveboard into safe zones based on the mean lateral deviation from the reference path and proximity to collision boundaries. Based on the zones, the system can determine if a correctional maneuver is needed to bring the driveboard into a low-risk coupling state. The simulation results guide in designing coupling strategies to achieve more reliable AMV operations.

1 INTRODUCTION

In recent times, Autonomous Modular Vehicles (AMVs) have attracted a lot of attention due to their high level of customizability. This customizability comes from separating the driving module from the transport capsule. The innovative design allows for flexible configurations to meet specific transportation needs and improve flexibility. One such innovative solution is the U-Shift vehicle concept developed by the Institute of Vehicle Concepts of the German Aerospace Center. The U-Shift consists of a capsule and a driveboard. The capsule is used for passenger transport or cargo delivery, while the driveboard is electrically powered and has all the essential driving components and systems (Osebek et al., 2025). This modular, automated, electric transportation system is built to use fewer driveboards and more interchangeable capsules. The driveboard has a unique "U" shape that allows it to hold the capsule between its arms. It also has a height-adjustable suspension system that lifts the capsule, as shown in Figure 1.

The attachment process between the driveboard and the capsule, which is called the coupling process, is defined and simulated in this paper. The first step involves determining the position and orientation of the capsule in relation to the driveboard and planning a suitable path. The second step focuses on controlling the driveboard to follow this path. In normal driving mode, the driveboard is operated with front-wheel steering. However, since the entire coupling maneuver is predominantly executed in reverse, the control system must steer the vehicle as if it had rear-wheel steering. In this situation, maintaining precise control is essential. Any misalignment or error during the coupling process could make both the driveboard and the capsule unusable until fixed.

Figure 1: The Concept of U-Shift Vehicle (Ulrich et al., 2023).

Automated coupling presents several key challenges: (1) achieving accurate localization of the capsule, particularly critical as the driveboard nears the capsule; (2) designing a precise path that minimizes

[a] https://orcid.org/0009-0007-3700-4274

Mysore Pavan, R. S.
Achieving Reliable U-Shift Capsule Coupling: A Comparative Study of Geometric Steering Controllers and Safe Operating Zone Determination.
DOI: 10.5220/0014696700004030

In *Proceedings of the 12th International Conference on Vehicle Technology and Intelligent Transport Systems (VEHITS 2026)*, pages 235-243
ISBN: 978-989-758-831-0; ISSN: 2184-495X

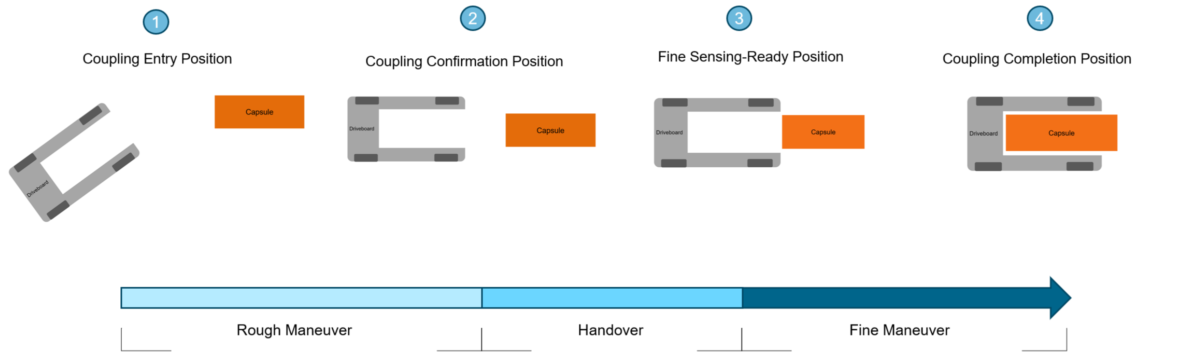

Figure 2: Chronological Coupling Positions and Phases Between the Driveboard and Capsule. The Simulation and Control Analysis Focus on the Fine Maneuver, but the Derived Maps Guide the Handover Phase Decision.

execution errors and allows potential fault correction; (3) developing a control strategy capable of reliably tracking the planned path. In this paper, we assume that the exact position and orientation of the capsule relative to the driveboard are known. The focus is on path planning and steering control. The longitudinal velocity is assumed to be low enough that dynamic effects are negligible and can later be scheduled along the path to satisfy steering and dynamic constraints. The following sections detail the methodology, including system design. This is followed by simulation-based testing, presentation of results, and concluding remarks with directions for future research.

2 METHODOLOGY

The coupling is defined in four stages that follow a chronological order with the possibility of stepwise validation and error containment in each phase as shown in Figure 2. It begins with the Coupling Entry Position, where the driveboard performs an initial approach maneuver to the capsule that does not require high positional accuracy. This is followed by the Coupling Confirmation Position, where alignment should be verified to ensure that the system is within a safe tolerance for the next steps. Next, the Fine Sensing Ready Position needs high-resolution sensors to take over, helping in precise control as the driveboard nears the capsule. Finally, in the Coupling Completion Position, the driveboard executes millimeter-level corrections to achieve secure mechanical and functional coupling. This progression from coarse to precise control facilitates accuracy and safety at each stage of the process. The positions are aligned with three operational phases: Rough Maneuver, Handover, and Fine Maneuver. The rough maneuver is characterized by higher tolerances in perception accuracy and control, whereas the fine maneuver requires stricter tolerances. The Handover phase bridges rough and fine control, ensuring the system is sufficiently aligned and within tolerance limits. To ensure stable vehicle maneuvering, steering dynamics play a crucial role in guiding the vehicle along curved paths. At low speeds, vehicles exhibit a kinematic behavior governed by Ackermann conditions, allowing slip-free movement (Jazar, 2025). The Ackermann steering facilitates that all wheels turn freely without slipping by aligning their motion with the instantaneous center of rotation (O), as illustrated in Figure 3.

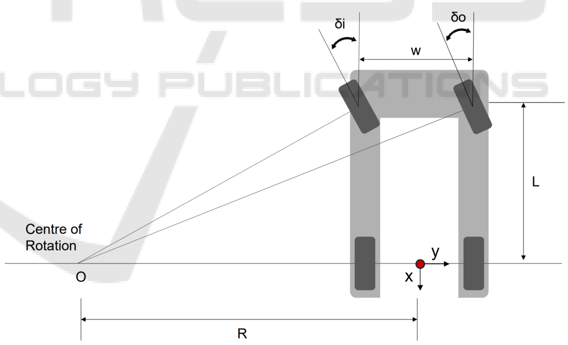

Figure 3: Driveboard and Kinematic Condition.

Although most vehicles on the market do not strictly follow the perfect Ackermann steering geometry, it is generally accepted that at very low speeds, the Ackermann condition applies. At these speeds, tire slip angles get close to zero (Jazar, 2025). The slip angle α can be expressed as

$$\alpha = \arctan\left(\frac{V_y}{V_x}\right), \tag{1}$$

as described in (1.183) of (Jazar, 2025). Here, V_x and V_y denote the contact-patch velocity components resolved in the tire-fixed local coordinates: x_t is aligned with the wheel plane and y_t points to the left of the wheel. For steered wheels, this frame is rotated by the steer angle δ relative to the vehicle frame. This corresponds to the small-angle form of the general definition $\alpha = \text{atan2}(V_y, V_x)$. When V_y becomes negligible in relation to V_x at low speeds, the ratio $\frac{V_y}{V_x}$ tends to zero and thus $\alpha \to 0$, justifying the assumption of the Ackermann condition.

In vehicles with ideal Ackermann steering geometry, the minimum turning radius can be derived from the relationship between the inner wheel steering angle, wheelbase, and front track width. For the inner wheel at maximum steer angle δ_{in}, the instantaneous center of rotation (ICR) lies along the extension of the rear axle centerline. The turning radius to the rear axle midpoint is given by

$$R = \frac{L}{\tan(\delta_{in})} + \frac{T}{2} \qquad (2)$$

where L is the wheelbase and T is the front track width. Substituting $L = 2.65\,\text{m}$, $T = 2.00\,\text{m}$, and $\delta_{in} = 25^\circ$ yields $R \approx 6.68\,\text{m}$. This formulation establishes the prerequisite for both inner and outer wheels to roll without lateral slip, which is a fundamental condition in Ackermann steering design (Gillespie, 1992). The study (Kong et al., 2015) suggests that kinematic vehicle models perform well at low speeds and moderate lateral accelerations, providing simplicity and ease of implementation due to the minimal parameter requirements. In contrast, dynamic vehicle models are computationally intensive and require detailed parameter identification, but offer higher fidelity during high-speed or aggressive maneuvers. Considering the low-speed nature and localized scope of the coupling maneuver, this study uses the kinematic bicycle model, implemented in MATLAB through the bicycleKinematics object (The MathWorks, Inc., 2024d). This formulation balances model simplicity and computational efficiency while capturing the essential geometric relationship between vehicle motion, wheelbase, and steering input.

2.1 Planner

The vehicle exhibits non-holonomic behavior, meaning it cannot instantaneously move sideways due to kinematic constraints such as steering angle limitations and the inability of wheels to slip laterally. These constraints restrict the vehicle's motion, allowing it to move only forward or backward along paths determined by its orientation. Hybrid A*, as introduced by Dolgov et al. (Dolgov et al., 2008), combines discrete grid-based exploration with analytic Reed-Shepp curves for feasible path planning. The algorithm incrementally searches the continuous state space (x, y, θ), where each node represents a feasible vehicle configuration. From each node, a set of motion primitives—small forward and backward arcs respecting the vehicle's kinematics—is generated. Each motion is evaluated using a cost function that considers path length, steering effort, and proximity to obstacles. To accelerate convergence, Hybrid A* periodically attempts analytic expansions using Reed-Shepp curves that directly connect the current node to the goal, provided no collisions occur. This hybridization enables both efficient exploration and dynamically feasible path generation.

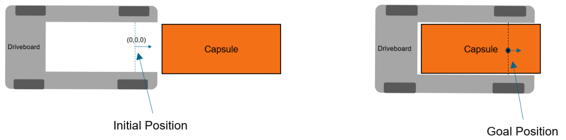

Figure 4: Initial and Goal Positions - Fine Maneuver.

Reed-Shepp curves inherently respect vehicle constraints, such as minimum turning radius and directional movements, enabling accurate heuristic estimation and significantly enhancing path feasibility while reducing positioning errors. The Fine Maneuver represents the most demanding scenarios for controllers, as it requires high accuracy in confined spaces. This study focuses specifically on such scenarios. The planner uses an initial reference point, specifically the center position of the driveboard rear axle, as shown in Figure 4, to generate the planned path. Subsequently, the controllers continue to reference this point throughout the maneuver, stabilizing and guiding the vehicle.

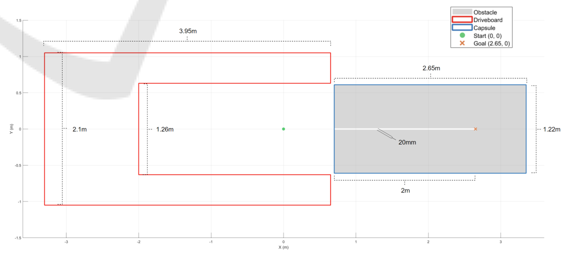

Figure 5: Top View with Driveboard, Capsule, and Obstacle with 20 mm Lateral Slit.

The center of the driveboard rear wheel axle moves inside the capsule during the coupling maneuver. At the start of the Fine Maneuver, the initial position is defined with a clearance of approximately 5 mm between the tip of the driveboard arm and the starting edge of the capsule. To enforce this constraint, the capsule is modeled as an obstacle with a 20 mm slit, as illustrated in Fig. 5, ensuring that the planner generates a path that fits within this space without exceeding its boundaries. The 20 mm width accounts for the ±10 mm tolerance, meaning that if the vehicle follows the planned path exactly, it remains within the allowable limit on the driveboard rail. This approach ensures the vehicle does not exceed the defined space. The coordinate system chosen for this study is a local fixed coordinate frame, with its origin defined at the initial position of the center of the rear axle of the driveboard at the start of the maneuver. This local reference point remains constant throughout the operation, which is suitable given the task's localized nature. A local map measuring 20×20 m is considered sufficient for effective planner execution.

2.2 Controller

Controllers play a critical role in ensuring that a vehicle follows its intended path. The choice of controller depends primarily on the system's specific requirements and the limits of real-time performance. Based on (Rokonuzzaman et al., 2021), the motion control task can be classified into two categories: (i) stabilization with respect to a reference point and (ii) stabilization with respect to a reference manifold. While stabilization to a reference point addresses discrete point-to-point movements, stabilization with respect to a reference manifold enables continuous path-following and tracking. In the context of U-Shift coupling, stabilization with respect to the planned path is superior, as it continuously minimizes lateral errors. Moreover, it provides greater flexibility during development, allowing for defined tolerances in driveboard positioning. A range of control approaches exists, spanning from geometric steering controllers to nonlinear techniques. Model Predictive Control (MPC) is widely adopted in industry due to its ability to incorporate constraints and optimize performance. In this study, however, the focus is on two geometric steering controllers, Pure Pursuit and Stanley, which are selected for their simplicity and ease of implementation. In the Pure Pursuit controller, the control objective is achieved by continuously tracking a point located at a look-ahead distance (L_d) along the planned path. In this study, L_d is varied over a predefined range to determine the value that yields optimal steering performance. The steering angle is computed from the curvature of the circular arc connecting the current vehicle position to this look-ahead point. Figure 6a illustrates the geometric relationship between the vehicle, the look-ahead distance, and the goal point.

The control law is expressed as (Coulter, 1992):

$$\delta = \arctan\left(\frac{2L\sin\alpha}{L_d}\right) \tag{3}$$

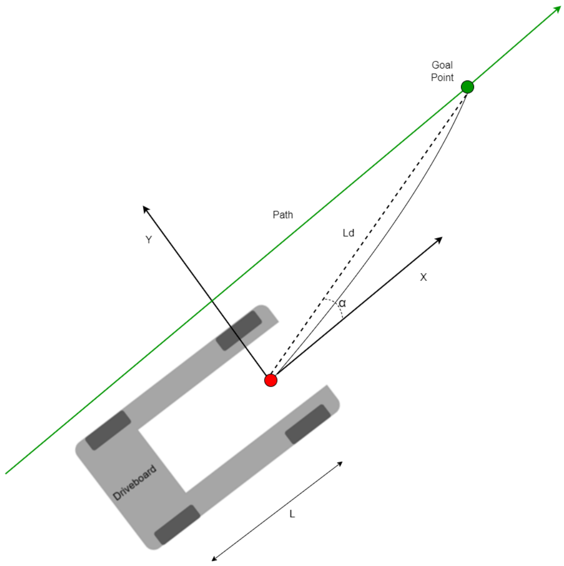

(a) Pure Pursuit geometric concept showing the look-ahead distance L_d, steering geometry, and heading angle α.

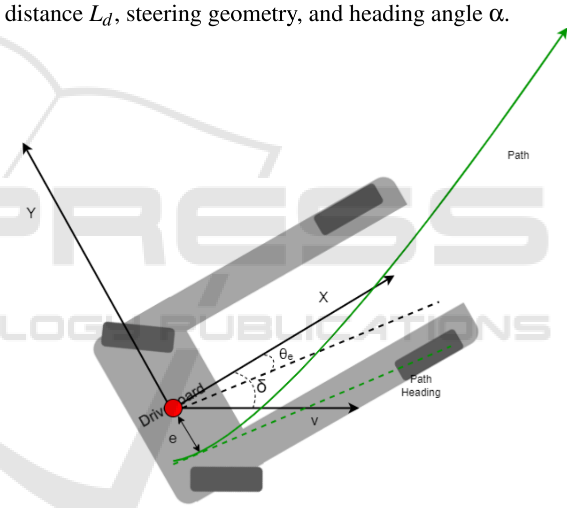

(b) Stanley control concept showing the cross-track error e, heading error ψ_e(with speed scaling).

Figure 6: Geometric path-tracking controllers: (a) Pure Pursuit and (b) Stanley controller with driveboard integration.

where:

- L is the wheelbase of the vehicle [m],
- α is the angle between the vehicle's heading and the line connecting the vehicle to the look-ahead point [rad],
- L_d is the look-ahead distance [m].

On the other hand, the Stanley controller minimizes lateral path deviation by combining two components: (i) a heading error term, which aligns the vehicle's heading with the path tangent, and (ii) a cross-track error term, which corrects lateral displacement from the path. The cross-track term is scaled by the

Table 1: Hybrid A* planner parameters.

Minimum turning radius	6.68	m
Motion primitive length	0.1	m

vehicle's speed, making the controller naturally stable at higher speeds but sensitive to tuning at low speeds. The control law includes a position gain that determines the influence of the cross-track error on the steering command. In this study, this gain is varied over a defined range to achieve a successful coupling with minimum mean lateral deviation. The control law is expressed as (Thrun et al., 2006):

$$\delta = \theta_e + \arctan\left(\frac{k \cdot e}{v}\right) \tag{4}$$

where:

- θ_e is the heading error between the vehicle's orientation and the path tangent (rad),
- e is the lateral cross-track error, i.e., perpendicular distance from the vehicle to the closest point on the path [m],
- k is the position gain,
- v is the vehicle's longitudinal velocity [m/s].

The vehicle velocity v is fixed at 0.1 m/s; therefore, only the scaling factor k/v remains constant, and the control law effectively behaves as a geometric formulation with a fixed proportional influence of the cross-track error. The values are selected based on the operational characteristics of the U-Shift driveboard, the physical constraints defined in the Hybrid A* planner, and the low-speed maneuvering requirements for the coupling scenario. The Stanley controller operates on the steering axle, typically the front axle. Although the reference path is generated for the rear-axle center, it is projected forward to the front-axle center for control. This ensures that the controller applies its steering law at the correct actuation point.

For the Pure Pursuit controller, the linear velocity is fixed at 0.1 m/s to reflect a safe docking speed, while the look-ahead distance (L_d) is varied over the range of 0.1 m to 1.5 m with a step size of 0.1 m to determine the value that ensures a successful coupling with minimum mean lateral deviation. The wheelbase of 2.65 m and the minimum turning radius of 6.68 m are defined according to the physical geometry of the vehicle and the Hybrid A* constraints (see Table 1). The motion primitive length, defined as the incremental distance the vehicle advances during each expansion step in the Hybrid A* search, is set to 0.1 m. This value defines the spatial resolution of the planner. The chosen value of 0.1 m provides a balanced compromise and is retained in the control layer to ensure consistency between planning and control. A simulation time step of 0.01 s is chosen to provide sufficient numerical resolution, and a steering tolerance of 1×10^{-2} rad is applied such that steering angle changes smaller than this threshold are ignored, preventing oscillatory corrections due to numerical noise.

For the Stanley controller, the linear velocity is also set to 0.1 m/s to maintain stability during low-speed gain variation tests. The wheelbase, minimum turning radius, and motion primitive length are kept identical to those in the Pure Pursuit configuration for comparison. The same simulation time step of 0.01 s is used to maintain consistency with the Pure Pursuit configuration. The position gain parameter k is varied in the range 1 : 1 : 10 purely to investigate whether a specific gain value could enable successful coupling.

3 SYSTEM DESIGN AND SIMULATION

The system architecture developed for the lateral controller analysis is illustrated in Figure 7. The design comprises four major functional components: obstacle map creation, path planning, lateral controller, and vehicle model. Initially, the capsule's position is defined and used to generate an occupancy grid map of the obstacle environment. This map is then provided to the Hybrid A* planner, implemented in MATLAB using the plannerHybridAStar function (The MathWorks, Inc., 2024c). The planner computes a collision-free path from the initial vehicle pose to the target position, while respecting the driveboard's kinematic constraints. The resulting planned path is subsequently provided as input to the lateral controller.

In this study, two lateral controllers are considered for path tracking: MATLAB controllerPurePursuit and the Lateral Controller Stanley (The MathWorks, Inc., 2024a) (The MathWorks, Inc., 2024b). Each controller is simulated independently to evaluate its performance in generating steering commands for the driveboard. In both cases, a constant longitudinal velocity is assumed, thereby reducing the problem to lateral guidance and control. The resulting steering angle, combined with the constant velocity input, is applied to the driveboard model to update the motion.

The driveboard model is represented by the MATLAB bicycleKinematics formulation, which captures the geometric relationships between driveboard motion, steering input, and wheelbase. The model is

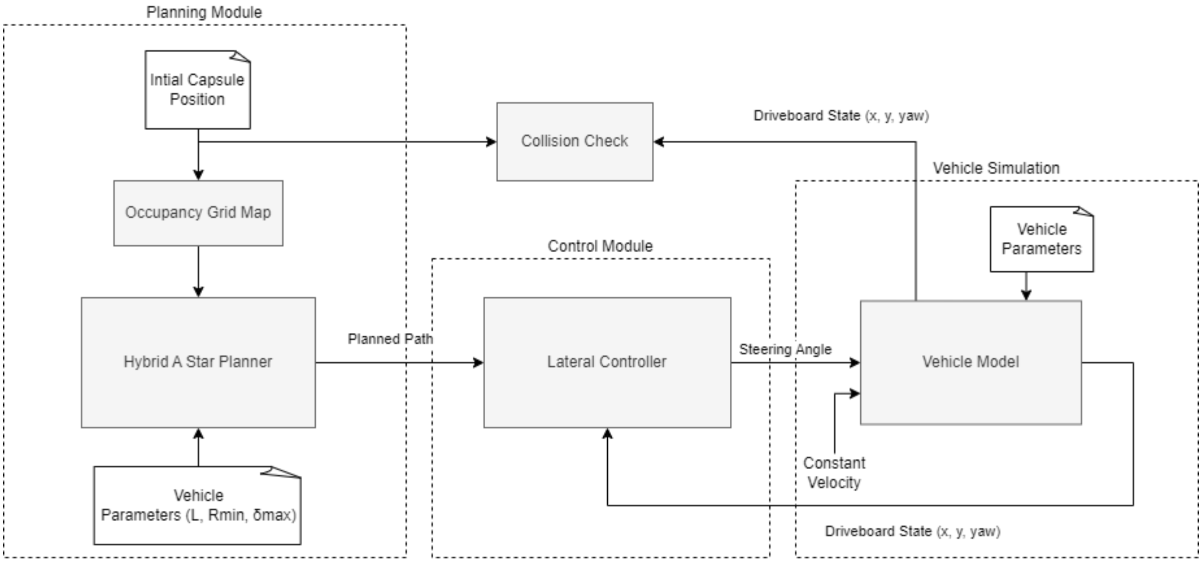

Figure 7: System overview for lateral controller analysis using MATLAB's Hybrid A (plannerHybridAStar), lateral controllers (controllerPurePursuit, lateralControllerStanley), and vehicle model (bicycleKinematics).

parameterized using the geometric properties of the driveboard, such as wheelbase length, which are supplied through the vehicle parameters block. The model simulates the evolution of the driveboard position and orientation as it follows the commanded path.

A closed-loop feedback structure is employed in which the updated driveboard pose is continuously fed back to the lateral controller and the collision-check module. In the present implementation, the Hybrid A planner is executed once at initialization to generate a feasible reference path. The lateral controller then operates in closed loop with the driveboard model to minimize path deviation. At the same time, the collision check module records whether a collision occurs for a given initial lateral and angular offset. Upon detection of a collision, the current simulation run is terminated, the event is logged for analysis, and the framework automatically proceeds to the next set of initial parameters. A coupling is considered successful when the driveboard reaches the goal position along the vehicle's x-axis without making contact with the capsule; otherwise, it is regarded unsuccessful. In all simulations, the initial setup includes a 5 mm gap between the tip of the driveboard arm and the starting edge of the capsule, providing a consistent starting condition for every run. The analysis focuses on the Fine Maneuver, as this stage places the highest demands on precision and often reveals the limitations of the controllers.

4 RESULTS

Figures 8a and 8d present collision maps comparing the coupling success rates of the Pure Pursuit and Stanley controllers. Red indicates a failed coupling maneuver and black denotes a successful one. In Figure 8a, the Hybrid A* planner is used with a minimum turning radius of 6.68 meters and a motion primitive length of 0.1 meters. The Pure Pursuit controller is applied by sweeping the look-ahead distance (L_d) from 0.1 m to 1.5 m in steps of 0.1 m with a constant longitudinal velocity of 0.1 m/s. Among all simulated L_d values, the one yielding the minimum mean lateral deviation is recorded. If at least one look-ahead distance value results in successful coupling, the corresponding case is classified as a no-collision scenario.

Figure 8d is generated using the Hybrid A* planner with the same motion primitive length and minimum turning radius. The Stanley controller is applied with a position gain range of 1–10 (step size 1) and constant longitudinal velocity of 0.1 m/s. Of all simulated position gain values, the one with the minimum mean lateral deviation is recorded. This result is then visualized on the maps. If even one position-gain value leads to a successful coupling, that case is marked as a no-collision scenario. For this comparative analysis, the test space was intentionally defined by sweeping the initial lateral offset y from -0.02 m to 0.02 m and the initial angular offset θ from $-3°$ to $3°$. This initial operational envelope defines the Total Domain Area (0.24 in arbitrary units used for comparison). The Feasible Area (or collision-free

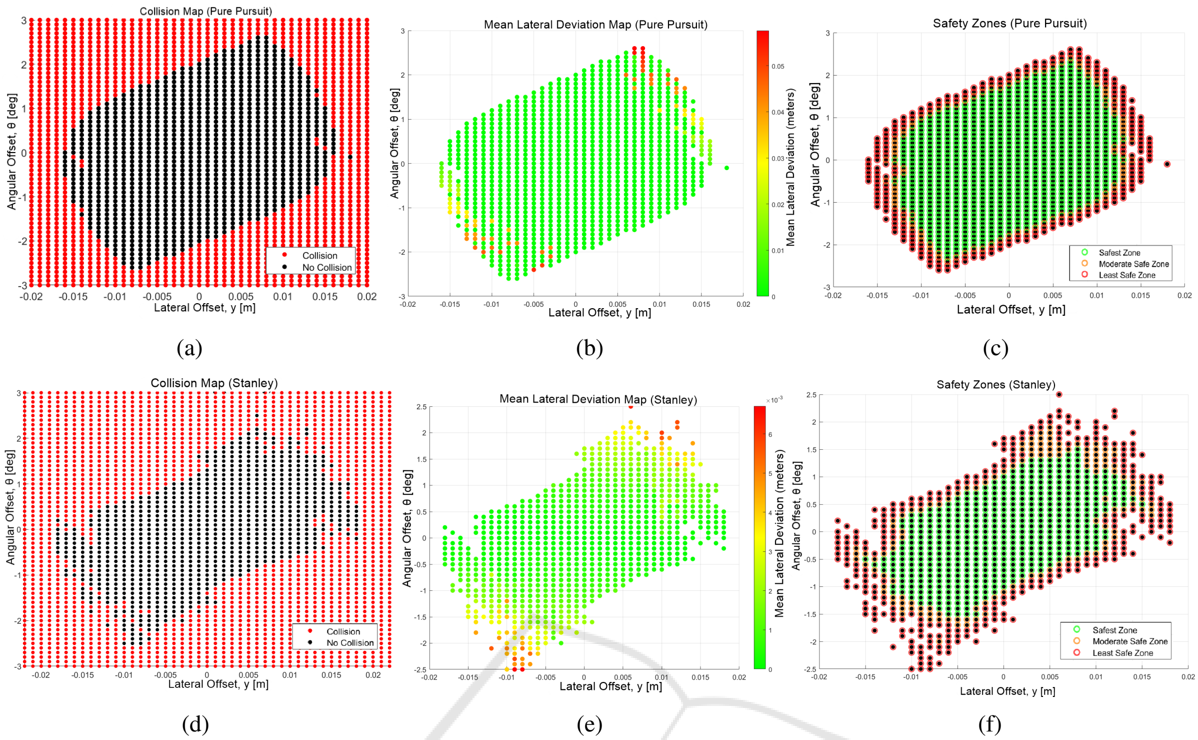

Figure 8: (A) Collision Map from Hybrid A* Planner using the Pure Pursuit Controller with a Bicycle Kinematic Vehicle Model, (b) Mean Lateral Deviation Map (Pure Pursuit), (c) Safety Zones (Pure Pursuit) (d) Collision Map from Hybrid A* Planner using the Stanley Controller with a Bicycle Kinematic Vehicle Model, (e) Mean Lateral Deviation Map (Stanley), (f) Safety Zones (Stanley).

area) corresponds to the total area represented by successful, no-collision coupling maneuvers (black dots) within this predefined domain. The overall robustness of each controller against initial alignment errors is quantified using the Feasibility Ratio R, which normalizes the successful operational space and is defined in (5).

$$R = \frac{\text{Feasible Area}}{\text{Total Domain Area}} \tag{5}$$

The collision map shows the natural symmetry of the driveboard and the capsule. This creates a roughly symmetric distribution, though not perfect. Isolated no-collision points can be identified at the edges of the no-collision areas. These isolated points are likely caused when the steering controller (Stanley or Pure Pursuit) is able to recover or manage the path deviation for one specific combination of initial offset and orientation but fails immediately when that initial offset is even slightly shifted. An additional point of interest is the mean lateral deviation of the driveboard relative to the reference path. Specifically, for a given longitudinal position, this deviation is defined as the difference between the lateral coordinate of the reference path and the simulated lateral position of the driveboard at that longitudinal position. Figures 8b and 8e present the minimum mean lateral deviations in all successful coupling scenarios. This analysis provides insights into the regions where adjustments to the initial position and orientation of the capsule and driveboard should be prioritized to achieve more deterministic and consistently successful coupling.

Figure 9 shows the optimal look-ahead distance (L_d) selected for the Pure Pursuit controller across different initial lateral and angular offsets, obtained by sweeping L_d from 0.1, m to 1.5, m and minimizing the mean lateral deviation under successful coupling conditions. It can be observed that scenarios with larger lateral and/or angular offsets require longer look-ahead distances, while near-nominal alignment conditions favor shorter look-ahead values, enabling faster convergence. Figure 11 maps the optimal position gain selected for the Stanley controller across different initial lateral and angular offsets. The gain was selected from values between 1 and 10. Selection was based on minimizing the mean lateral deviation in successful, collision-free coupling scenarios. The results show that moderate to high position gain values are preferred over a wide range of initial conditions. In particular, a position gain of 10 is selected most frequently. This trend is consistent with Figure 10, which relates the position gain to the achieved minimum mean lateral deviation. Higher gain values are more frequently associated with lower lateral deviation for scenarios with smaller initial lateral and angular errors.

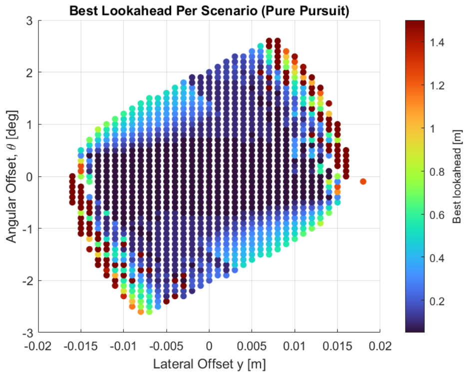

Figure 9: Best Look-ahead Distance for Pure Pursuit Controller.

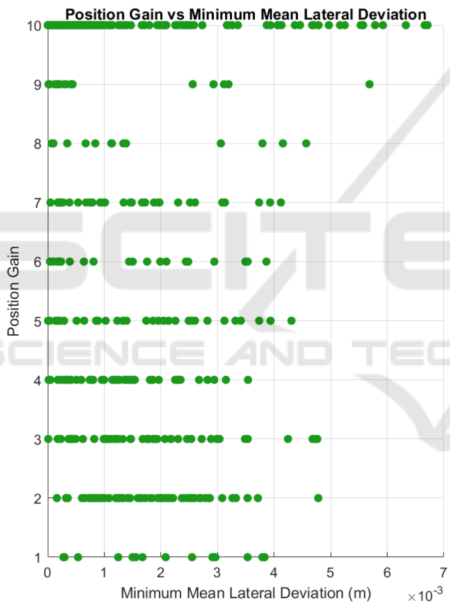

Figure 10: Stanley Controller Position Gain vs Minimum Mean Lateral Deviation.

The safety zones shown in Figures 8c and 8f are derived from the lateral deviation maps by classifying the offsets according to their relative proximity to the collision boundaries. Edge positions and orientations are automatically marked as least safe, as they are closest to potential collisions. The safest zone is defined when the lateral deviation is $\leq 45\%$ of the maximum deviation, while the moderate safe zone extends up to 80%; all remaining states are classified as least safe.To improve robustness, a neighborhood connectivity check is used. This requires each state to meet minimum-neighbor requirements at successive

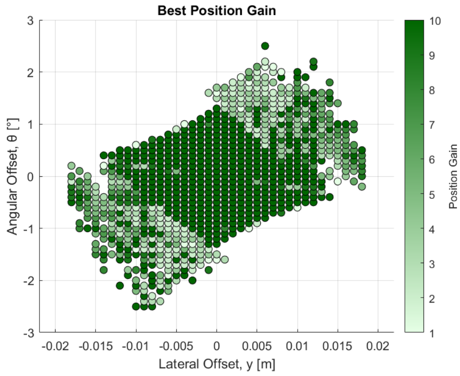

Figure 11: Stanley Controller Best Position Gain.

levels of adjacency (4-neighbor logic). This process ensures that isolated safe points are reclassified according to the consistency of their local surroundings. At the transition between the Rough and Fine Maneuver, based on this map, the system can decide whether a correction maneuver is needed to bring the driveboard's position and orientation to lower-risk points.

5 CONCLUSION

Based on collision, lateral deviation, the optimal initial orientation of the driveboard and capsule can be determined by identifying regions that are collision-free and exhibit minimal lateral deviation. While the Pure Pursuit controller tolerates lateral offsets of approximately ± 0.017 m and angular deviations up to $\pm 2.6°$, the measured data indicate that it covers a larger feasible area, with a feasibility ratio of 0.464 (feasible area: 0.1114, total domain area: 0.24). Outside of its collision-free band, the controller rapidly loses tracking performance, leading to collision. In contrast, the Stanley controller covers a smaller feasible region, with a feasibility ratio of 0.359 (feasible area: 0.0862, total domain area: 0.24), while tolerating initial lateral offsets of up to ± 0.018 m and angular deviations up to $\pm 2.3°$. Importantly, the Stanley controller consistently achieves a lower mean lateral deviation, with values remaining below approximately 0.007 m, indicating higher tracking precision. Furthermore, the mean lateral deviation achieved by the Pure Pursuit controller is not significantly better and, in several cases, is worse, offering no precision advantage over the Stanley controller. The safety maps show that Pure Pursuit attains a larger safety area, with approximately 44% more "Safest Zones" samples than Stanley, which exhibits narrower safest regions and reduced tolerance to positional errors.

Overall, the results reveal a fundamental trade-off between coverage and precision, suggesting a context-dependent control strategy for reliable coupling. The Pure Pursuit controller is the optimal choice for the Handover phase, where the priority is the robustness to initial positioning errors due to its superior feasibility ratio and its larger "Safest Zone" compared to Stanley. To ensure minimum lateral errors, L_d should be dynamically selected from the Best Look-ahead map based on the current driveboard state. Longer L_d is optimum for larger offsets, and shorter L_d for near alignment to achieve faster convergence. However, for the Fine Maneuver, the system should switch to the Stanley controller to take advantage of its superior tracking precision. For this phase, the results indicate that a high position gain (k=10) is more effective, as this value is most frequently associated with the minimum mean lateral deviation in successful scenarios without collision.

For the driveboard, the current study uses a kinematic bicycle model, which is appropriate at low speeds where vehicle dynamics can be ignored. In order to improve the overall fidelity of vehicle representation and capture subtle dynamic effects, even at low speeds, future work can expand the analysis to dynamic vehicle models. Additionally, the simulations only require lateral guidance and control because they maintain a constant longitudinal velocity of 0.1 m/s. In future work, longitudinal velocity scheduling and alternative or hybrid control strategies that can handle both longitudinal and lateral motion at the same time could be investigated. Additionally, these techniques could be tested and verified on real U-Shift driveboard prototype to verify if the simulation-derived safety zones hold true under actual sensor noise and surface conditions.

ACKNOWLEDGEMENTS

This work is conducted at the Institute of Vehicle Concepts, DLR Stuttgart, supported by the MAD Urban project and funded by the German Federal Ministry for Economic Affairs and Energy (BMWE). Special thanks to Dr.-Ing. Tilman Bünte and Jürgen Weimer for reviewing the paper and providing helpful suggestions.

REFERENCES

Coulter, R. C. (1992). Implementation of the pure pursuit path tracking algorithm. Technical Report CMU-RI-TR-92-01, Carnegie Mellon University, Pittsburgh, PA.

Dolgov, D., Thrun, S., Montemerlo, M., and Diebel, J. (2008). Practical search techniques in path planning for autonomous driving. *AAAI Workshop - Technical Report*.

Gillespie, T. D. (1992). *Fundamentals of Vehicle Dynamics*. Society of Automotive Engineers.

Jazar, R. N. (2025). *Vehicle Dynamics: Theory and Application*. Springer Cham, Cham, 4 edition. Published: 07 January 2025, Pages: XXVII, 1167.

Kong, J., Pfeiffer, M., Schildbach, G., and Borrelli, F. (2015). Kinematic and dynamic vehicle models for autonomous driving control design. In *2015 IEEE Intelligent Vehicles Symposium (IV)*, pages 1094–1099. IEEE.

Osebek, M., Scheibe, S., Münster, M., and Siefkes, T. (2025). Evolution and safety concept of the modular u-shift vehicle for sustainable mobility of people and goods. In McNally, C., Carroll, P., Martinez-Pastor, B., Ghosh, B., Efthymiou, M., and Valantasis-Kanellos, N., editors, *Transport Transitions: Advancing Sustainable and Inclusive Mobility*, pages 562–568, Cham. Springer Nature Switzerland.

Rokonuzzaman, M., Mohajer, N., Nahavandi, S., and Mohamed, S. (2021). Review and performance evaluation of path tracking controllers of autonomous vehicles. *IET Intelligent Transport Systems*, 15(5):646–670.

The MathWorks, Inc. (2024a). controllerpurepursuit (robotics system toolbox) [documentation]. https://www.mathworks.com/help/robotics/ref/controllerpurepursuit-system-object.html. Retrieved August 16, 2025.

The MathWorks, Inc. (2024b). Lateral controller stanley (automated driving toolbox) [documentation]. https://www.mathworks.com/help/driving/ref/lateralcontrollerstanley.html. Retrieved August 16, 2025.

The MathWorks, Inc. (2024c). plannerhybridastar (navigation toolbox) [documentation]. https://www.mathworks.com/help/nav/ref/plannerhybridastar.html. Retrieved August 16, 2025.

The MathWorks, Inc. (2024d). *Robotics System Toolbox: bicycleKinematics*. Accessed: 2025-08-16.

Thrun, S., Montemerlo, M., Dahlkamp, H., Stavens, D., Aron, A., Diebel, J., Fong, P., Gale, J., Halpenny, M., Hoffmann, G., Lau, K., Oakley, C., Palatucci, M., Pratt, V., Stang, P., Strohband, S., Dupont, C., Jendrossek, L.-E., Koelen, C., and Mahoney, P. (2006). Stanley: The robot that won the darpa grand challenge. *J. Field Robotics*, 23:661–692.

Ulrich, C., Feinauer, M., Bieber, K., Schmid, S. A., and Friedrich, H. E. (2023). Life cycle analysis of an on-the-road modular vehicle concept. *Sustainability*, 15(13).